

Estimating demosaicing algorithms using image noise variance

Jun Takamatsu

Nara Institute of Science and Technology
MSR-IJARC fellow
8916-5, Takayama-cho, Ikoma, Nara, Japan

j-taka@is.naist.jp

Tsukasa Ogasawara

Nara Institute of Science and Technology
8916-5, Takayama-cho, Ikoma, Nara, Japan

ogasawar@is.naist.jp

Yasuyuki Matsushita

Microsoft Research Asia
5F, Beijing Sigma Center, No. 49, Zhichun road,
Haidian district, Beijing, China

yasumat@microsoft.com

Katsushi Ikeuchi

University of Tokyo
4-6-1, Komaba, Meguro-ku, Tokyo, Japan

ki@cvl.iis.u-tokyo.ac.jp

Abstract

We propose a method for estimating demosaicing algorithms from image noise variance. We show that the noise variance in interpolated pixels becomes smaller than that of directly observed pixels without interpolation. Our method capitalizes on the spatial variation of image noise variance in demosaiced images to estimate the color filter array patterns and demosaicing algorithms. We verify the effectiveness of the proposed method using various images demosaiced with different demosaicing algorithms extensively.

1. Introduction

Many consumer digital cameras are equipped with a square grid of photo-sensors overlaid with a color filter array (CFA). The color filters selectively allow light according to wavelength range to produce color information. Some digital cameras employ three separate sensors, each sensor taking a separate measurement of red, green, and blue by splitting light through a prism assembly. In single-sensor cameras, almost all of them use a *Bayer filter* on which each two-by-two submosaic contains two green, one blue, and one red filters. The raw image data captured by a sensor with a CFA is converted to a color image by a *demosaicing* algorithm. This process is illustrated in Figure 1 from right to left.

Precise understanding of imaging process is important for many computer vision algorithms that require accurate knowledge of irradiance. For the task of photometric calibration, there has been plenty of studies on estimation of camera response functions, vignetting, etc. Knowledge of the CFA pattern and the demosaicing algorithm is important

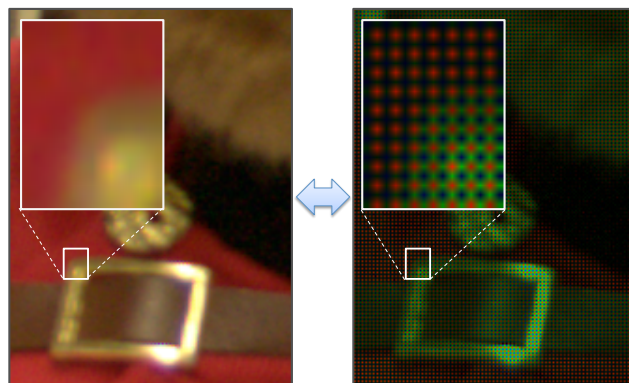


Figure 1. A color image (left) and the corresponding raw image (right). A demosaicing algorithm produces a color image from a raw image. Our method can invert the process of demosaicing.

as well to understand *true* irradiance; however, not many studies have been done in this direction. Since information on the CFA pattern and the demosaicing algorithm are typically not available from camera manufacturers, development of an estimation algorithm is important.

In this paper, we develop a method for automatically determining CFA patterns and demosaicing algorithms. We refer to a CFA pattern to indicate the arrangement of the submosaic color filter pattern at a particular location on the sensor. We use a physical property of the image noise variance, *i.e.*, it becomes smaller after interpolation, to determine the interpolated pixels. After CFA estimation, our method further estimates the demosaicing algorithm using the distribution of interpolation weights. The overview of the proposed method is illustrated in Figure 2.

This paper has two major contributions. First, we show

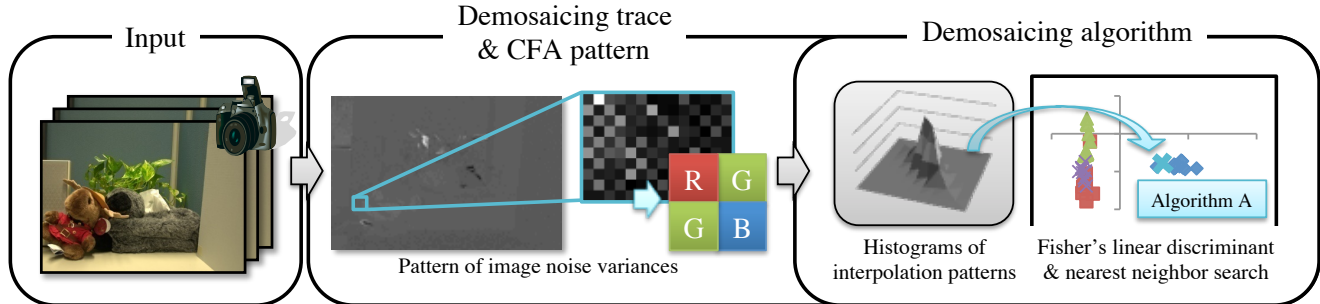


Figure 2. Overview of the proposed method. Our method takes registered color images or a single color image as input. Our method consists of three stages: 1) detection of the demosaicing trace, 2) estimation of the CFA pattern, and 3) estimation of the demosaicing algorithm.

how the image noise variance is skewed by the demosaicing process; the noise variance of interpolated pixels becomes smaller than that of the directly observed pixels. Second, we develop a method to automatically identify CFA patterns and demosaicing algorithms from the distribution of noise variances.

2. Prior work

Demosaicing aims to produce high-quality color images while avoiding the introduction of false color artifacts (*e.g.*, chromatic aliases, zippering, etc.) at low computational cost. There have been many studies on demosaicing algorithms. A recent survey by Liu *et al.* covers a wide variety of state-of-the-art demosaicing algorithms [12].

Recent demosaicing algorithms are far more complex than straightforward interpolation methods such as nearest-neighbor/bilinear interpolation methods. Since the Bayer pattern has more green pixels than either red or blue pixels, many demosaicing algorithms first interpolate the green colors for better edge preservation, and later resample the red and the blue colors. For edge preservation, Chang *et al.* [2] proposed to interpolate pixel values based on the magnitude of the image gradient. Hirakawa and Parks [7] selected the best value among the pre-computed candidates based on the criterion of image naturalness. Tsai and Song proposed an efficient selection method that avoids heavy computation of the candidate colors [20].

Estimation of the demosaicing algorithms has been studied in the context of digital forensics. Popescu and Farid [15, 16] used the EM algorithm for identifying a demosaicing algorithm. Bayram *et al.* proposed a method for classifying digital camera models from information about camera-specific interpolation [1]. Gallagher proposed a method for detecting linear or cubic interpolation using the periodicity of the second order derivatives of the interpolated images [5]. Gallagher and Chen presented a method for distinguishing natural images from photo realistic computer-graphics images using demosaicing traces [6].

Our work is also related to image noise analysis in physics-based computer vision. Image noise has been actively used for vision algorithms in previous approaches. For example, Liu *et al.* [11] developed a method for estimating noise level function from a single image and used it for efficient image denoising. Matsushita and Lin [13] used image noise for defining accurate intensity similarity measure. Hwang *et al.* [9] proposed a noise-robust edge detection algorithm based on noise observations. Treibitz and Schechner [19] theoretically proved the recovery limits in point-wise degradation considering intensity-dependent image noise effects.

In another stream of image noise analysis in computer vision, there are methods that perform estimation only from noise observations. Matsushita and Lin [14], and Takamatsu *et al.* [17, 18] have shown that image noise provides sufficient information for estimating radiometric response functions. Like their methods that use the image noise as signal, our method estimates the trace of the demosaicing and the CFA pattern only from noise observations.

3. Demosaicing and image noise

This section describes the relationship between image noise variance and color interpolation in a demosaicing process. Specifically, we show that the noise variance of interpolated pixels tends to become smaller than that of the directly observed pixels. In the following, we call the directly observed pixel value as observed intensity to differentiate it from interpolated intensity.

In the demosaicing process, the intensity $I_I(\mathbf{p})$ of an interpolated pixel \mathbf{p} is obtained by combining the observed intensities $I_O(\mathbf{q})$ of the neighboring pixels \mathbf{q} for each color channel. This process can be formulated as Eq. (1), where $R_{\mathbf{p}}$ represents the set of the observed pixels that are located near pixel \mathbf{p} .

$$I_I(\mathbf{p}) = \sum_{\mathbf{q} \in R_{\mathbf{p}}} w(\mathbf{q}; \mathbf{p}) I_O(\mathbf{q}). \quad (1)$$

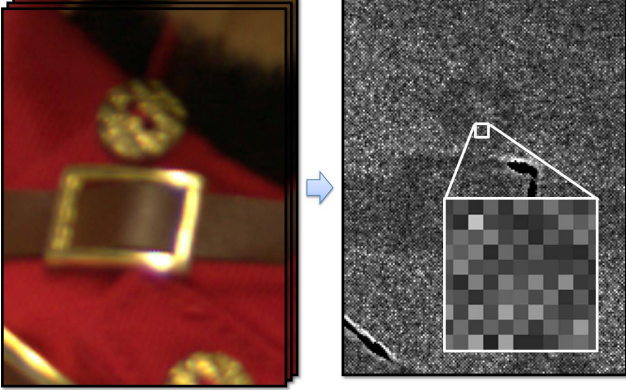


Figure 3. Visualization of image noise variances of the G-channel (right) computed from registered images (left). Variances of pixels whose values are obtained by interpolation tend to be smaller. The visible checker pattern corresponds to the Bayer pattern.

Note that subscripts I and O denote interpolated and observed pixels, respectively.

Let us now consider how image noise variance is altered through the demosaicing process. Here we assume that the observed image noise is spatially independent. An intensity $I(\mathbf{p})$ in a demosaiced image can be described by the noise-free intensity $\tilde{I}(\mathbf{p})$ and the image noise $N(\mathbf{p})$ as

$$I(\mathbf{p}) = \tilde{I}(\mathbf{p}) + N(\mathbf{p}). \quad (2)$$

Substituting Eq. (2) into Eq. (1), we obtain

$$N_I(\mathbf{p}) = \sum_{\mathbf{q} \in R_{\mathbf{p}}} w(\mathbf{q}; \mathbf{p}) N_O(\mathbf{q}), \quad (3)$$

because \tilde{I}_I is canceled out by the weighted sum of \tilde{I}_O in Eq. (3). From Eq. (3), the image noise variance can be described as

$$\begin{aligned} \sigma_I^2(\mathbf{p}) &= \sum_{\mathbf{q}, \mathbf{r} \in R_{\mathbf{p}}} w(\mathbf{q}; \mathbf{p}) w(\mathbf{r}; \mathbf{p}) \text{cov}(N_O(\mathbf{q}), N_O(\mathbf{r})) \\ &= \sum_{\mathbf{q} \in R_{\mathbf{p}}} w(\mathbf{q}; \mathbf{p})^2 \sigma_O^2(\mathbf{q}), \end{aligned} \quad (4)$$

where $\sigma_I^2(\mathbf{p})$ and $\sigma_O^2(\mathbf{q})$ represent the variances of $N_I(\mathbf{p})$ and $N_O(\mathbf{q})$, respectively. And $\text{cov}(N_O(\mathbf{q}), N_O(\mathbf{r}))$ represents the covariance between $N_O(\mathbf{q})$ and $N_O(\mathbf{r})$. Because of the spatial independence of the noise distributions,

$$\text{cov}(N_O(\mathbf{q}), N_O(\mathbf{r})) = 0, \quad \mathbf{q} \neq \mathbf{r}.$$

Let us take a simple example to illustrate. Consider the case of bilinear interpolation, $w(\mathbf{q}; \mathbf{p}) = 1/n$ for all \mathbf{q} where n is the number of elements in the set $R_{\mathbf{p}}$. Substituting $w(\mathbf{q}; \mathbf{p}) = 1/n$ into Eq. (4), we obtain

$$\sigma_I^2(\mathbf{p}) = \frac{1}{n} \bar{\sigma}_O^2(\mathbf{p}),$$

where $\bar{\sigma}_O^2(\mathbf{p})$ is the average variance of the neighboring observed pixels $R_{\mathbf{p}}$. From this result, it is naturally expected that the variance at the interpolated pixel becomes smaller. Figure 3 shows the visualization of image noise variance of the G-channel that is computed from registered color images. In the figure, a checker-board pattern can be clearly seen, which corresponds to the Bayer pattern.

We use the decreasing tendency of the noise variance of the interpolated pixels to determine the CFA pattern. Also, this tendency weakens when either 1) weights of interpolation, or 2) the noise variance distribution in the neighboring observed pixels are very biased. However, these two conditions seldom occur in practice.

4. Estimation method

Our estimation method consists of the following steps: 1) detection of the demosaicing trace, 2) estimation of the CFA pattern, and 3) estimation of the demosaicing algorithm. To obtain image noise variance, multiple registered images with fixed camera parameters and view position are usually used. The image noise variance is obtained from the fluctuated values at the corresponding pixels across the images. While a large number of images is preferred statistically, our method fortunately works well with just the rough estimates of the variance. Therefore, it only requires a few images (five images in this paper). In this section, we will describe the algorithms of the above steps. We assume that the possible candidates for CFA patterns are known in advance because the types of CFA patterns (*e.g.* Bayer filters) are limited in practice.

4.1. Detection of the demosaicing trace

Consider a 1D sequence of noise variances where the variances of the interpolated and the observed pixels alternately appear. Applying the discrete Fourier transform (DFT) to the sequence, the DFT magnitude is maximized when the frequency ω equals to π , because the interpolated and the observed variances appear by turns. This DFT property is also used by Gallagher and Chen [6], but we use noise variance as input instead of the derivatives of the color images. Given a hypothesized CFA pattern, our method assigns labels (interpolated or observed) to pixels. Then, we apply DFT as mentioned above and evaluate the magnitude. When the hypothesized CFA pattern is correct, the DFT magnitude becomes large. We test for every possible hypothesis.

To construct the 1D sequence of variances, we take the average of the variances in the interpolated pixels along the diagonal path of submosaics. The same procedure is performed on the observed pixels. Using many diagonal paths, we obtain a set of average variances of the interpolated and the observed pixels. Finally, a long 1D sequence of vari-

ances is obtained by arranging them. The reason why we sample variances diagonally is to avoid JPEG compression artifacts. Since JPEG compression is applied to each 8×8 pixel block, horizontal or vertical arrangement generates other peak frequencies [5].

By applying DFT to the 1D sequence $\{x_k\}$, the Fourier series $\{f_j\}$ in the frequency domain is obtained as

$$f_j = \sum_{k=0}^{m-1} x_k e^{-\frac{2\pi i}{m} jk} \quad (j = 0, \dots, m-1), \quad (5)$$

where m is the length of the sequence. Similar to the method of [6], we define the criterion C_1 for determining whether there exists a trace of demosaicing as

$$C_1 = \frac{|f_{mid}|}{|f_{m/2}|}, \quad (6)$$

where $f_{m/2}$ is the $m/2$ -th element of the Fourier series. Its norm $|f_{m/2}|$ is the amplitude of $(m/2)$ -Hz wave, and f_{mid} is the element whose amplitude is the median of all the amplitudes $\{|f_j|\}$.

This value C_1 becomes smaller if the hypothesized CFA pattern is plausible. If the criterion C_1 is larger than a predefined threshold τ for all possible CFA patterns, we consider that as the absence of demosaicing trace.

4.2. Estimation of the CFA pattern

The method described in Section 4.1 is effective for finding CFA patterns as well as trace of demosaicing. However, periodicity can be observed even when an incorrect CFA pattern is assumed. To solve this problem, we use an additional criterion for estimating the CFA pattern.

We define a simple criterion C_2 for the estimation that assesses the plausibility of the hypothesized CFA pattern as

$$C_2 = \frac{\bar{\sigma}_O^2}{\bar{\sigma}_I^2}, \quad (7)$$

where $\bar{\sigma}_I^2$ and $\bar{\sigma}_O^2$ are the average variances of all the interpolated pixels and that of observed pixels, respectively. The larger C_2 is, the more likely the hypothesized CFA pattern is. This criterion C_2 can be computed in each color channel. We use all color channels to make the criterion robust by summing them up as

$$C_3 = C_2^R + C_2^G + C_2^B, \quad (8)$$

where C_2^R , C_2^B , and C_2^G are the C_2 criteria in the RGB channels.

One weakness of this criterion C_3 is that it is more sensitive to JPEG compression artifacts than the criterion C_1 . JPEG compression contaminates the pixel values regardless of observed and interpolated pixels. As a result, the difference between the maximum and the second maximum of

the criterion C_1 becomes small as JPEG compression ratio becomes high. Therefore, if the difference in C_1 is larger than a predefined threshold (we used 0.5 in this paper), we consider JPEG compression ratio to be low enough and use C_3 criterion. Otherwise, we use C_1 criterion.

4.3. Estimation of the demosaicing algorithm

To estimate the demosaicing algorithm, we use the histogram of the interpolation weights $w(\mathbf{q}; \mathbf{p})$. Representing Eq. (1) in a vector form, we obtain

$$\mathbf{I}_O^T \mathbf{w} = I_I(\mathbf{p}) \quad (9)$$

at each interpolated pixel \mathbf{p} . We use notation $R_{\mathbf{p}}$ to represent the set of pixels that are used for the interpolation ($R_{\mathbf{p}} \stackrel{\text{def}}{=} \{\mathbf{q}_1, \dots, \mathbf{q}_n\}$), where n is the number of the neighboring observed pixels. The observed pixel intensities \mathbf{I}_O and interpolation weights \mathbf{w} are represented in a vector form as $\mathbf{I}_O^T = (I_O(\mathbf{q}_1), \dots, I_O(\mathbf{q}_n))^T$ and $\mathbf{w}^T = (w(\mathbf{q}_1; \mathbf{p}), \dots, w(\mathbf{q}_n; \mathbf{p}))^T$. We can obtain many samples for Eq. (9) from many locations in the image coordinates. For each \mathbf{p} , we can create a set of equations of Eq. (9) using multiple registered images. With conditions

$$\sum_{\mathbf{q} \in R_{\mathbf{p}}} w(\mathbf{q}; \mathbf{p}) = 1, \quad \text{and}$$

$$\forall \mathbf{p}, \mathbf{q}, 0 \leq w(\mathbf{q}; \mathbf{p}) (\leq 1), \quad (10)$$

we estimate the interpolation weights \mathbf{w} by solving the linear system of equations in a least-squares manner.

We use Fisher's linear discriminant (FLD) [4] and nearest-neighbor search for the classification of the demosaicing algorithms. Given the input feature, the classifier finds the nearest class in the FLD subspace.

To generate the training dataset, we first calculate interpolation weight vectors \mathbf{w} from images demosaiced by a certain demosaicing algorithm. Then, the weight vector \mathbf{w} is computed at every interpolated pixel location. Depending on the pixel location, the length of weight vectors \mathbf{w} varies. Next, we create a histogram of the weight vectors \mathbf{w} for each length of the weight vectors. Finally, these histograms are normalized and concatenated to obtain a single vector form of the training data. The same procedure is applied for creating other training data representing a different demosaicing algorithm.

Note that the order of elements in the weight vector does not have much meaning from the view point of the interpolation method. For example, the weight vector (0.4, 0.6) is regarded to be the same as the weight vector (0.6, 0.4). Therefore, we just sort the vector elements in ascending order.

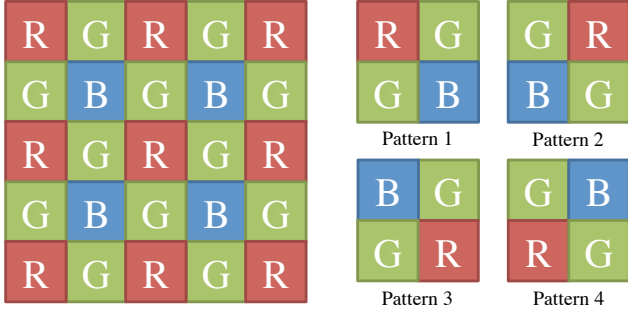


Figure 4. Bayer pattern and possible two-by-two submosaic patterns.

4.4. Estimation from a single image

The accurate estimation of image noise variance requires multiple registered images of the same scene. It is often too demanding, because such a dataset is not available in practice. To relax the condition, we assume that the irradiance of the neighboring pixels is similar, and that variance can be computed using the group of neighboring pixels. A similar assumption was also used in previous work (*e.g.*, [17]), although in a different context. Since the characteristics of noise variances in interpolated and observed pixels are different, we create the pixel groups by using only the same class of pixels (either interpolated or observed).

In the single-image case, when the number of observed pixels which are used for interpolation, *i.e.*, elements in the set $R_{\mathbf{p}}$, is more than three, the available constraints are insufficient to uniquely determine interpolation weights \mathbf{w} at pixel \mathbf{p} . This is because we only have two constraints, Eqs. (9) and (10). In the multiple-image case, this does not become a problem since we can create more equations from multiple registered images. To resolve this ill-posedness in the single-image case, we use an additional condition to regulate the solution. To avoid excessive deviation, we define the condition that the sum of squared weights is minimized: $\min \mathbf{w}^T \mathbf{w}$.

5. Experiments

In this section, we evaluate the proposed method in two scenarios: the multiple-image case and the single-image case. We also assess the robustness of the algorithm against JPEG compression.

5.1. Multiple-image case

Setup In this experiment, we assume four local types of the Bayer pattern as candidate CFA pattern as shown in Figure 4, like most of the demosaicing algorithms [12]. We use the neighbor set $R_{\mathbf{p}}$, which consists of four neighboring pixels in the G-channel and two or four pixels in R/B-

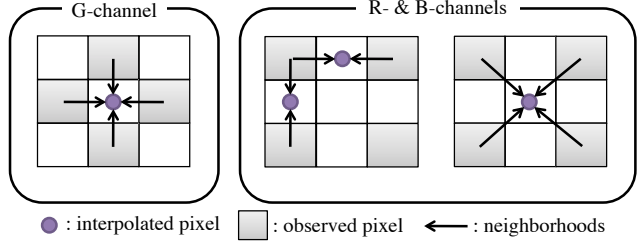


Figure 5. Definition of neighborhoods in interpolation. The circle indicates the interpolated pixel and the gray block indicates the observed pixel. The arrow shows the neighbor relationship.

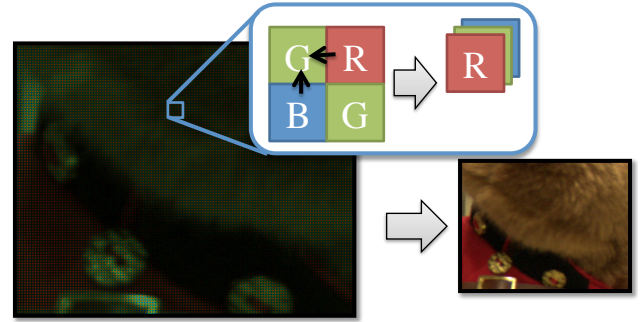


Figure 6. Construction of non-interpolated images by down-sampling using only the observed pixels.

channels for each \mathbf{p} (see Figure 5). The threshold τ is empirically set to $\tau = 0.1$ throughout the experiment.

To prepare the ground truth dataset, we captured five registered RAW images for each of 18 different scenes (four scenes taken by EOS kiss digital original version, seven scenes by EOS kiss digital N, seven scenes by EOS 20D). The captured RAW images are converted to color images by six different demosaicing algorithms implemented in *dcrw* [3] and *RAW THERAPEE* [8]. These are bilinear, variable number of gradients (VNG) [2], patterned pixel grouping (PPG) [10], and adaptive homogeneity-directed (AHD) [7] algorithms implemented in *dcrw*, and Horváth's AHD (EAHD) and Heterogeneity-Projection Hard-Decision (HPHD) [20] algorithms of *RAW THERAPEE*.

We also created color images without demosaicing interpolation by directly down-sampling RAW images as shown in Figure 6. In down-sampling, every 2×2 submosaic of the RAW image produces only one color pixel. We include this as one of the demosaicing algorithm. In the following, this data is referred to as *non-interpolated*, since demosaicing algorithms generally use some interpolation. Therefore we have seven demosaicing algorithms in total. After demosaicing, we applied JPEG compression to the demosaiced images for assessing the robustness against JPEG compression. Figure 7 shows example of the images used for the



Figure 7. Example of images used for the experiment.

experiment. We use the half of all the images as a training set, and the other half as a testing set.

When creating histograms of the weight vectors w , we set the size of the histogram bin to be one tenth of $1/n$ where n is the number of observed neighbors for interpolation, because each element in w spans in the range of $[0, 1/n]$. Using FLD, the histograms of w were projected into a compact 4-D subspace.

Demosaicing trace The first row in Table 1 shows the accuracy of the detection of the demosaicing trace by the proposed method. The accuracy is evaluated with different JPEG compression qualities. *True positive* indicates the rate of the correct answer for demosaiced inputs. On the other hand, *True negative* is the rate of the correct answer for non-interpolated inputs. When JPEG quality is greater than 90, the accuracy of the proposed method is also high (over 95-percent). Because JPEG compression tends to uniformly increase noise variance in the entire image, the periodicity of noise variances used for detection is relatively maintained. For this reason, performance degradation of the proposed method against JPEG compression is not significant.

CFA pattern The second row in Table 1 shows the estimation accuracy of CFA patterns against JPEG compression. Note that we did not use the image set of which the demosaicing trace could not be detected. As described above, JPEG compression contaminates the pixel values regardless of observed and interpolated pixels, and therefore it smooths out the difference between the observed and the interpolated pixels. As a result, the information of CFA pattern is buried as the compression ratio becomes higher.

Once the CFA pattern is estimated, we can produce an irradiance image before demosaicing within an 8-bit accuracy. Figure 4 shows an example of reversing the demosaicing process. The Bayer pattern image (right) is computed from the input image (left) using our method.

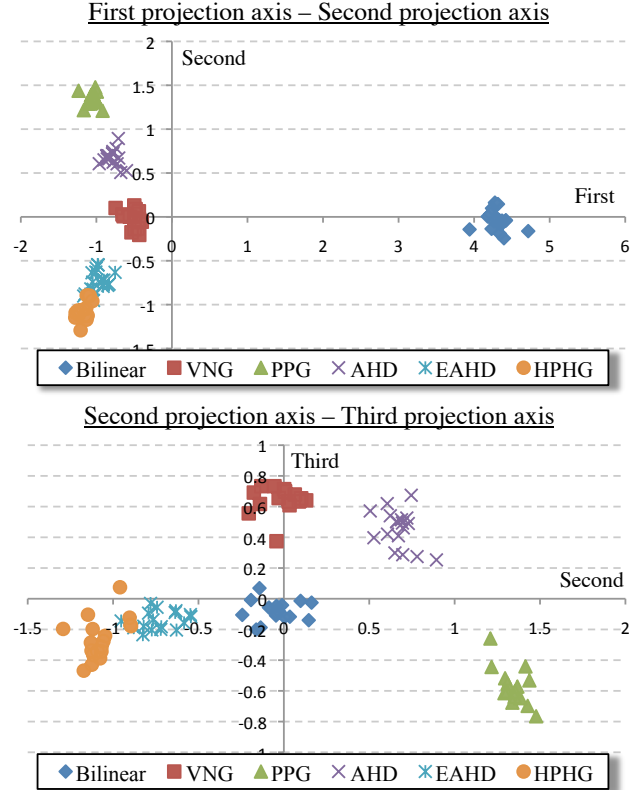


Figure 8. Plots of vectors which represent histogram of interpolation weight, in the feature space. They are visualized by projection onto the 2-D plane using Fisher's linear discriminant analysis [4]. Different demosaicing algorithms form distinct clusters in the features.

Demosaicing algorithm The third column in Table 1 shows the estimation accuracy of the demosaicing algorithm against JPEG compression. Our method performs accurately when the compression ratio is low. However, it is affected by the JPEG quality; accuracy decreases with loss of quality. This is due to the fact that the compression contaminates the pixel values randomly, which makes it difficult to robustly estimate the interpolation weights.

Figure 8 shows the 2-D plots of all the image sets in the FLD space. Since the bilinear interpolation is very distinct from other demosaicing algorithms, the FLD's first projection separates the bilinear interpolation compared to others. The other distributions also show clear distinction from each other in the higher-order projection.

5.2. Single image case

For the single-image case, we used 32 images for the experiment. The right-hand side of Table 1 shows the accuracy of all the steps in the single-image case. The robustness against JPEG compression is very similar to that of the multiple-image case.

Table 1. Quantitative evaluation of our method in the multiple-image case and single-image case. From top to bottom, results of 1) detection of the demosaicing trace, 2) estimation of the CFA pattern, and 3) estimation of the demosaicing algorithm are shown. From left to right, the accuracy is evaluated with various JPEG qualities (100 indicates no compression).

	JPEG quality	Multiple images				Single image			
		100	98	95	90	100	98	95	90
Demosaicing trace	True positive [%]	100	100	99.1	96.3	100	100	94.8	90.1
	True negative [%]	100	100	100	100	100	100	96.9	75.0
CFA pattern	Accuracy [%]	95.8	92.6	73.1	63.0	98.4	94.3	89.6	83.3
Demosaicing algorithm	Accuracy [%]	89.8	78.5	70.5	53.8	96.2	94.0	88.9	75.8

Table 2. Accuracy of the estimation of demosaicing algorithms. Comparison between the proposed method and Popescu and Farid’s method [16] are shown.

	JPEG quality			
	100	98	95	90
The proposed method	94.6	88.6	79.6	63.1
Popescu and Farid	91.5	73.4	69.3	64.1

5.3. Comparison

We compare our method with previous approaches. In this comparison, we use the same dataset used for the single-image case (Section 5.2).

Detection of demosaicing trace We compared the proposed method with Gallagher and Chen’s method [6]. Figure 9 shows ROC curves of the two methods in the cases where JPEG quality is 70 and 90. This result shows the proposed method is slightly superior to the method [6], even though our method only uses noise information.

Estimation of demosaicing algorithm We compared the proposed method with Popescu and Farid’s method [16]. Popescu and Farid’s method assumes that the input to their algorithm is a demosaiced image but does not perform the detection of demosaicing trace. Therefore, we used only demosaiced images as input to these two methods. Because their method estimates the algorithm without the knowledge of the CFA pattern, we regarded the failure of estimating CFA patterns as the failure of estimating the demosaicing algorithm in our method, *i.e.*, the recognition accuracy is computed as the product of the accuracy of the CFA pattern recognition and the accuracy of the demosaicing algorithm recognition.

Table 2 shows the result with various degrees of JPEG compression. Our method performs well when the JPEG compression artifact is not significant. As the compression artifact becomes stronger, the accuracy of both methods goes down.

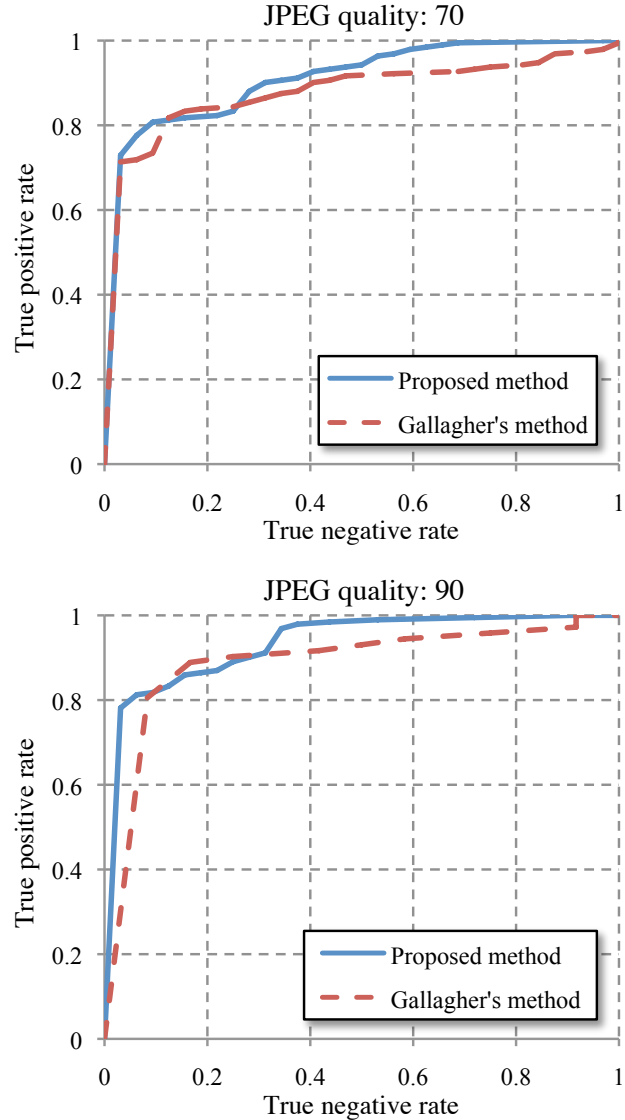


Figure 9. Detection rate of demosaicing traces. ROC curves of the proposed method and Gallagher and Chen’s method [6] are shown for the cases of JPEG quality 70 and 90.

6. Discussions

In this paper, we showed the relationship between image noise variance and demosaicing. We have developed an algorithm for estimating CFA patterns and demosaicing algorithms. Extensive quantitative evaluation was performed to verify the effectiveness of the proposed method. Nevertheless, our method has some limitations, and there are several avenues for future work.

One limitation of our method is that the accuracy goes down when the image is processed after demosaicing, *e.g.*, image compression and other image filtering. These image processing operations significantly alter the noise distribution in unpredictable manner. It is very likely that explicitly accounting for these factors can increase the applicability of the proposed method. We are investigating the possibility of deciphering such post-processing operations using the observation of image noise. Another direction for future work is to apply the proposed method as a pre-processing stage for various vision tasks. Because interpolated pixels are essentially synthetically produced pixels, identifying the pixels that really receive irradiance (not by interpolation) is important for physics-based vision methods.

Acknowledgement

This work is supported by Microsoft Institute for Japanese Academic Research Collaboration (MS-IJARC).

References

- [1] S. Bayram, H. T. Sencar, and N. Memon. Classification of digital camera-models based on demosaicing artifacts. *Digital Investigation*, 5:49–59, 2008. 2
- [2] E. Chang, S. Cheung, and D. Y. Pan. Color filter array recovery using a threshold-based variable number of gradients. In *Proc. of SPIE, Sensors, Cameras, and Applications for Digital Photography*, volume 3650, pages 36–43, 1999. 2, 5
- [3] D. Coffin. <http://www.cybercom.net/~dcoffin/dcrawl/>. 5
- [4] R. A. Fisher. The use of multiple measurement in taxonomic problems. *Annals of Eugenics*, 7:179–188, 1936. 4, 6
- [5] A. C. Gallagher. Detection of linear and cubic interpolation in jpeg compressed images. In *Proc. of Canadian Conf. on Comp. and Robot Vis.*, pages 65–72, 2005. 2, 4
- [6] A. C. Gallagher and T. Chen. Image authentication by detecting traces of demosaicing. In *Proc. of CVPR Workitorial on Vision of the Unseen*, 2008. 2, 3, 4, 7
- [7] K. Hirakawa and T. W. Parks. Adaptive homogeneity-directed demosaicing algorithm. *IEEE Trans. Image Processing*, 14:360–369, 2005. 2, 5
- [8] G. Horváth. <http://www.rawtherapee.com/>. 5
- [9] Y. Hwang, J.-S. Kim, and I.-S. Kweon. Sensor noise modeling using the skellam distribution: Application to the color edge detection. In *Proc. of Comp. Vis. and Patt. Recog. (CVPR)*, 2007. 2
- [10] C.-K. Lin. <http://web.cecs.pdx.edu/~cklin/demosaic/>. 5
- [11] C. Liu, W. T. Freeman, R. Szeliski, and S. B. Kang. Noise estimation from a single image. In *Proc. of Comp. Vis. and Patt. Recog. (CVPR)*, pages 901–908, 2006. 2
- [12] X. Liu, B. Gunturk, and L. Zhang. Image demosaicing: A systematic survey. In *SPIE the Int'l Society for Optical Engineering*, 2008. 2, 5
- [13] Y. Matsushita and S. Lin. A probabilistic intensity similarity measure based on noise distribution. In *Proc. of Comp. Vis. and Patt. Recog. (CVPR)*, 2007. 2
- [14] Y. Matsushita and S. Lin. Radiometric calibration from noise distributions. In *Proc. of Comp. Vis. and Patt. Recog. (CVPR)*, 2007. 2
- [15] A. C. Popescu and H. Farid. Exposing digital forgeries by detecting traces of re-sampling. *IEEE Trans. on Signal Processing*, 53(2):758–767, 2005. 2
- [16] A. C. Popescu and H. Farid. Exposing digital forgeries in color filter array interpolation images. *IEEE Trans. on Signal Processing*, 53(10):3948–3959, 2005. 2, 7
- [17] J. Takamatsu, Y. Matsushita, and K. Ikeuchi. Estimating camera response functions using probabilistic intensity similarity. In *Proc. of Comp. Vis. and Patt. Recog. (CVPR)*, 2008. 2, 5
- [18] J. Takamatsu, Y. Matsushita, and K. Ikeuchi. Estimating radiometric response functions from image noise variance. In *Proc. of European Conf. on Comp. Vis. (ECCV)*, 2008. 2
- [19] T. Treibitz and Y. Y. Schechner. Recovery limits in pointwise degradation. In *Proc. of IEEE Int. Conf. on Computational Photography*, 2009. 2
- [20] C.-Y. Tsai and K.-T. Song. Heterogeneity-projection hard-decision color interpolation using spectral-spatial correlation. *IEEE Trans. on Image Processing*, 16(1):78–91, 2007. 2, 5